Lysosome-dependent Ca2+ release response to Fas activation in coronary arterial myocytes through NAADP: evidence from CD38 gene knockouts

Fan Zhang, Min Xia and Pin-Lan Li

Am J Physiol Cell Physiol 298:1209-1216, 2010. First published Mar 3, 2010;
doi:10.1152/ajpcell.00533.2009

Am J Physiol Cell Physiol 298: C1209–C1216, 2010.
First published March 3, 2010; doi:10.1152/ajpcell.00533.2009.

Lysosome-dependent Ca^{2+} release response to Fas activation in coronary arterial myocytes through NAADP: evidence from CD38 gene knockouts

Fan Zhang, Min Xia, and Pin-Lan Li

Department of Pharmacology and Toxicology, Medical College of Virginia, Virginia Commonwealth University, Richmond, Virginia

Submitted 4 December 2009; accepted in final form 26 February 2010

Zhang F, Xia M, Li PL. Lysosome-dependent Ca^{2+} release response to Fas activation in coronary arterial myocytes through NAADP: evidence from CD38 gene knockouts. *Am J Physiol Cell Physiol* 298: C1209–C1216, 2010. First published March 3, 2010; doi:10.1152/ajpcell.00533.2009.—Activation of the death receptor Fas has been implicated in the development of vascular injury or disease, but most studies have focused on its role in the regulation of cell apoptosis and growth. The present study was designed to examine the early response of coronary artery to Fas activation by its ligand, FasL. The hypothesis being tested is that CD38 signaling pathway mediates FasL-induced intracellular Ca^{2+} release through nicotinic acid adenine dinucleotide phosphate (NAADP) in mouse coronary arterial myocytes (CAMs) and thereby produces vasoconstriction in coronary arteries. HPLC analysis demonstrated that FasL markedly increased NAADP production in CAMs from wild-type mice ($CD38^{+/+}$) but not in cells from CD38 knockout ($CD38^{-/-}$) mice. Using fluorescent Ca^{2+} imaging analysis, we found that FasL (10 ng/ml) significantly increased Ca^{2+} release from 142.5 ± 22.5 nM at the basal level to 509.4 ± 64.3 nM in $CD38^{+/+}$ CAMs but not in $CD38^{-/-}$ CAMs. However, direct delivery of NAADP, the CD38 metabolite, into $CD38^{-/-}$ CAMs still markedly increased Ca^{2+} release, which could be significantly attenuated by a lysosomal function inhibitor, bafilomycin A1 (Baf), or a NAADP antagonist, pyridoxal-phosphate-6-azophenyl-2-disulfonic acid. Confocal microscopy further demonstrated that FasL produced a typical two-phase Ca^{2+} release with a local Ca^{2+} burst from lysosomes, followed by a global Ca^{2+} response in $CD38^{+/+}$ CAMs. In isolated perfused septal coronary arteries from $CD38^{+/+}$ mice, FasL was found to significantly increase U-46619-induced vasoconstriction from 29.2 ± 7.3 to 63.2 ± 10.3%, which was abolished by Baf (100 nM). These results strongly indicate that the early response of CAMs to FasL is to increase intracellular Ca^{2+} levels and enhance the vascular reactivity through stimulation of NAADP production and lysosome-associated two-phase Ca^{2+} release in coronary arteries.

death receptor ligand; second messenger; vasomotor response; vascular smooth muscle

IT IS WELL KNOWN THAT INTRACELLULAR Ca^{2+} plays a critical role in the regulation of smooth muscle functions. Intracellular Ca^{2+} increase is either driven by Ca^{2+} influx across the plasma membrane or mobilized by Ca^{2+} messenger from Ca^{2+} storage organelles. So far, three intracellular Ca^{2+} messengers have been found: inositol 1,4,5-trisphosphate (IP_3), cyclic ADP-ribose (cADPR), and nicotinic acid adenine dinucleotide phosphate (NAADP). NAADP is the newly discovered and most potent intracellular universal Ca^{2+} messenger (26), which participates in the regulation of a wide variety of cell functions, such as fertilization, cell proliferation and differentiation, insulin secretion, and nitric oxide signaling (25), as well as vasoconstriction (43). In regard to the NAADP signal system, several reports have addressed the identity of NAADP-related Ca^{2+} stores and the characteristics of NAADP-sensitive Ca^{2+} release channels (5, 9, 41–42). In several cell types such as T-lymphocytes, cardiac cells, and skeletal muscle cells, NAADP has been proposed to target endoplasmic or sarcoplasmic reticulum (SR) Ca^{2+} store and to release Ca^{2+} via ryanodine receptors (RyRs) or a separate protein that may indirectly activate RyRs (13, 17). However, accumulating evidence has demonstrated that an NAADP-sensitive Ca^{2+} store is a thapsigargin-insensitive lysosome-like acidic store and that NAADP mobilizes Ca^{2+} from this NAADP-sensitive Ca^{2+} store to produce a local spatial Ca^{2+} signal, which triggers Ca^{2+}-induced Ca^{2+} release (CICR) to cause global Ca^{2+} increases through RyRs on the SR (11, 24, 43). This NAADP-mediated two-phase Ca^{2+} release response has been described in increasing cell types such as sea urchin egg, pancreatic cells, and hepatocytes, as well as smooth muscle cells (4, 10, 43). Regarding the NAADP enzymatic pathway, *Aplysia* ADP-ribosyl cyclase and mammalian homologous CD38 have been reported as enzymes responsible for the synthesis of NAADP (1). Both CD38 and the cyclase synthesize NAADP from NADP by catalyzing the exchange of nicotinamide in NADP with nicotinic acid. Recently, it was reported that CD38 as a multifunctional enzyme also plays a critical role in the degradation of NAADP by hydrolyzing NAADP to ADP-ribose 2′-phosphate (18).

Fas ligand (FasL) is a type II transmembrane protein that belongs to the tumor necrosis factor (TNF) superfamily; it exists as a membrane molecule (mFasL) and also in a soluble form (sFasL) generated by metalloproteinase (MMP7) proteolytic cleavage. Apart from the proapoptotic activity against diverse cell types, the activation of Fas/FasL pathway also exerts a wide range of proinflammatory responses in different tissues, including the cardiovascular system (20, 23, 37–38). Recent studies have indicated that many inflammatory factors importantly affect the regulation of vascular function (23, 37–38). However, the mechanisms mediating the role of these inflammatory factors remain unknown. In this regard, it has been reported that increases in cytosolic Ca^{2+} concentration ($[Ca^{2+}]_i$) may mediate the action of FasL as an inflammatory factor. Given that Fas and FasL are ubiquitously expressed in the vasculature and the role of Ca^{2+} in the vasomotor response, we hypothesized that FasL-induced intracellular Ca^{2+} release via NAADP and lysosome in coronary arterial myocytes (CAMs) might participate in the inflammatory vasoconstriction in coronary arteries.

To test this hypothesis, we first characterized FasL-induced NAADP production in coronary arterial myocytes from both wild-type ($CD38^{+/+}$) and $CD38^{-/-}$ mice by HPLC analysis.

Address for reprint requests and other correspondence: P.-L. Li, Dept. of Pharmacology and Toxicology, Medical College of Virginia, Virginia Commonwealth Univ., 410 N 12th, Richmond, VA 23298 (e-mail: pli@vcu.edu).

We then addressed whether FasL induces Ca^{2+} release response in CAMs with fluorescence imaging technique in combination with an ultrasound microbubble intracellular delivery method. We also rescued the CD38 gene expression in $CD38^{-/-}$ CAMs by transfection of CD38 expression vector into the cells and examined whether the Ca^{2+} response could be restored. Using confocal microscopy, we further analyzed the NAADP-related two-phase Ca^{2+} release response to FasL and finally examined whether this FasL-induced two-phase Ca^{2+} release contributes to its vasomotor response in isolated mouse coronary artery.

MATERIALS AND METHODS

Genotyping $CD38^{-/-}$ mice. Both $CD38^{-/-}$ and wild-type mice were purchased from the Jackson Laboratory. All experimental protocols were reviewed and approved by the Animal Care Committee of Virginia Commonwealth University. In $CD38^{-/-}$ homozygous mice, a genomic fragment of exons 2 and 3, which encodes CD38 putative active site, was replaced by a neomycin selection cassette. PCR confirmation of this genotype was achieved by specific primers designed for wild-type extron 2, 5′-TCTGAGGACCAATGTTAGGATG-3′ and 5′-CTAATGGAACTTCGCCTTGTG-3′, and for the neomycin selection cassette in $CD38^{-/-}$, 5′-CTTGGGTGGAGAGGCTATTC-3′ and 5′-AGGTGAGATGACAGGAGATC-3′. The genomic DNA was extracted from the mouse tail using the ArchivePure DNA purification kit (5 Prime), and the PCR reaction was carried out in a Bio-Rad iCycler, initiated at 94°C for 1 min to denature the template and activate the *Taq* DNA polymerase, followed by 30 cycles of PCR amplification. Each cycle included denaturing at 94°C for 30s, annealing at 55°C for 30s, and extension at 72°C for 1 min. The electrophoresis of PCR products was performed in 2% agarose gel. The expected 299-bp fragment for wild-type mouse and 280 bp for $CD38^{-/-}$ mouse was determined by comparing the DNA ruler.

HPLC analysis of NAADP conversion rate in CAMs. Mouse CAMs were isolated as described previously (36). The CAMs' identity was confirmed by immunocytochemical staining with anti-α-smooth muscle actin primary antibody (R&D Systems) and Alexa-Fluor 488-conjugated anti-mouse IgG secondary antibody (Invitrogen). Mouse endothelial cells were used as a negative control. To determine CD38-associated NAADP production, we measured base-exchange-related NAADP conversion using HPLC in CAMs from both wild-type and $CD38^{-/-}$ mice. Within a 100-μl reaction mixture, 1 mM $NADP^+$ and 30 mM nicotinic acid (NA) as substrates were added to 100 μg of cell homogenates in HEPES buffer containing (in mM) 20 HEPES, 1 EDTA, and 255 sucrose (pH 4.5). After incubation at 37°C for 30 min, the proteins were removed by centrifugation using an Amicon microultrafilter at 13,000 rpm for 15 min. The reaction product in the ultrafiltrate was then analyzed using HPLC as we described previously (43). Peak identities were confirmed by comigration, and absorbance spectra were compared with the known standards. Quantitative measurements were performed by comparison of known concentration of standards.

Fluorescence measurement of $[Ca^{2+}]_i$ and NAADP delivery in CAMs. Intracellular Ca^{2+} responses to FasL or NAADP were determined using a fluorescence image analysis system with the Ca^{2+} indicator fura-2 as described previously (19, 39). The Ca^{2+}-free Hanks' buffered saline solution (HBSS) including 1 mM EGTA was used for Ca^{2+} measurement to ensure the Ca^{2+} response was solely derived from intracellular Ca^{2+} store release rather than extracellular Ca^{2+} influx. HBSS contained (in mM) 137 NaCl, 5.4 KCl, 4.2 $NaHCO_3$, 3 Na_2HPO_4, 0.4 KH_2PO_4, 1.5 $CaCl_2$, 0.5 $MgCl_2$, 0.8 $MgSO_4$, 10 glucose, and 10 HEPES (pH 7.4). Administration of NAADP (1 μM) into the cells was carried out by wrapping this cell-impermeable nucleotide into Optison (Perflutren protein-type A microspheres) and by delivery with ultrasound as detailed previously (30, 35, 43).

CD38/green fluorescent protein plasmid transfection in CAMs. CD38 plasmid from OriGene was constructed by open reading frame cloning of full-length *Mus musculus* CD38 antigen (NM_007646) into pCMV6-AC-green fluorescent protein vector (pCD38-GFP). The transfection of pCD38-GFP into $CD38^{-/-}$ CAMs was achieved with the TransFectin protocol from Bio-Rad. pCMV6-AC-GFP without CD38 insert was used as a negative control. The transfection efficiency was determined by confocal microscopy as detection of the green fluorescence at 488-nm excitation and 510-nm emission.

Confocal fluorescence microscopic $[Ca^{2+}]_i$ measurement. Subconfluent CAMs in 35-mm cell culture dishes were loaded with the Ca^{2+}-sensitive dye fluo-4 (5 μM) in HBSS and then incubated at room temperature for 20 min. The fluo 4-loaded CAMs were then bathed with Ca^{2+}-free HBSS buffer containing 1 mM EGTA. To define intracellular stores responsible for FasL (10 ng/ml)-associated two-phase Ca^{2+} release, we pretreated the cells with bafilomycin A1 (Baf; 100 nM), a lysosome function inhibitor, or ryanodine (Rya; 50 μM), a SR Rya/Ca^{2+} antagonist. Ca^{2+} imaging was performed using a laser scanning confocal microscope (Olympus Fluoview System, version 5.0, FV300), which consists of an Olympus BX61WI inverted microscope with an Olympus Lumplan F1×60, 0.9 numerical aperture, and water-immersion objective. Ca^{2+}/fluo-4 fluorescence images were acquired at 488-nm excitation and >510-nm emission in the XYT recording mode with a speed of 2 frames/s. The Ca^{2+}/fluo-4 fluorescence intensity was analyzed with Fluoview version 5.0 software. The ratio of Ca^{2+}-dependent fluorescence intensity to that at basal level was quantified as the intracellular Ca^{2+} response.

Confocal fluorescence microscopic detection of lysosomes and Ca^{2+} colocalization. Subconfluent CAMs in 35-mm cell culture dishes were incubated with dextran-conjugated tetramethylrhodamine (Rho; 1 mg/ml; Molecular Probes) for 4 h in advanced DMEM medium containing 10% FBS at 37°C, 5% CO_2, followed by a 20-h chase in dye-free medium for lysosomes loaded with Rho (7). After being washed with HBSS buffer three times, the Rho-loaded cells were then incubated with the Ca^{2+}-sensitive dye fluo-4 at a concen-

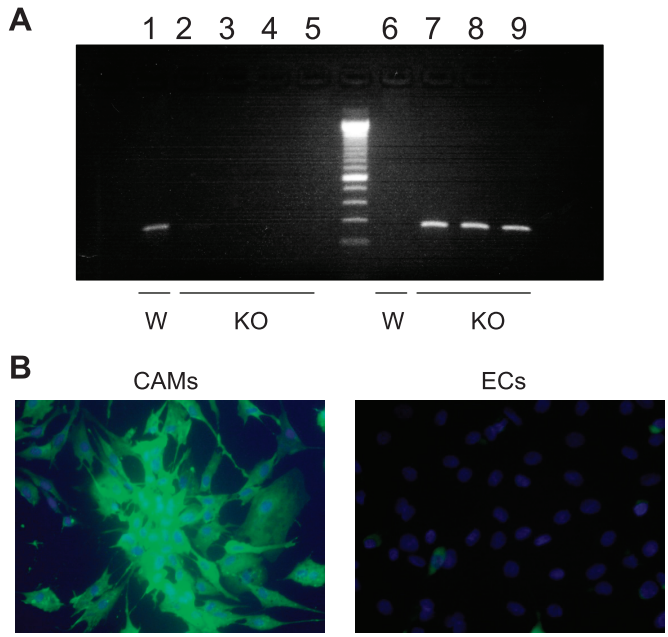

Fig. 1. Genotyping confirmation of wild-type (W) and CD38 knockout (KO) mice and identity determination of isolated coronary arterial myocytes (CAMs). *A*: a PCR product gel document from genotyping. See text for detailed description of lanes. *B*: CAM identity was confirmed by positive staining with anti-α-smooth muscle actin primary antibody and Alexa-Fluor 488-conjugated anti-mouse IgG secondary antibody (green stain), and negative control staining was shown in endothelial cells (ECs).

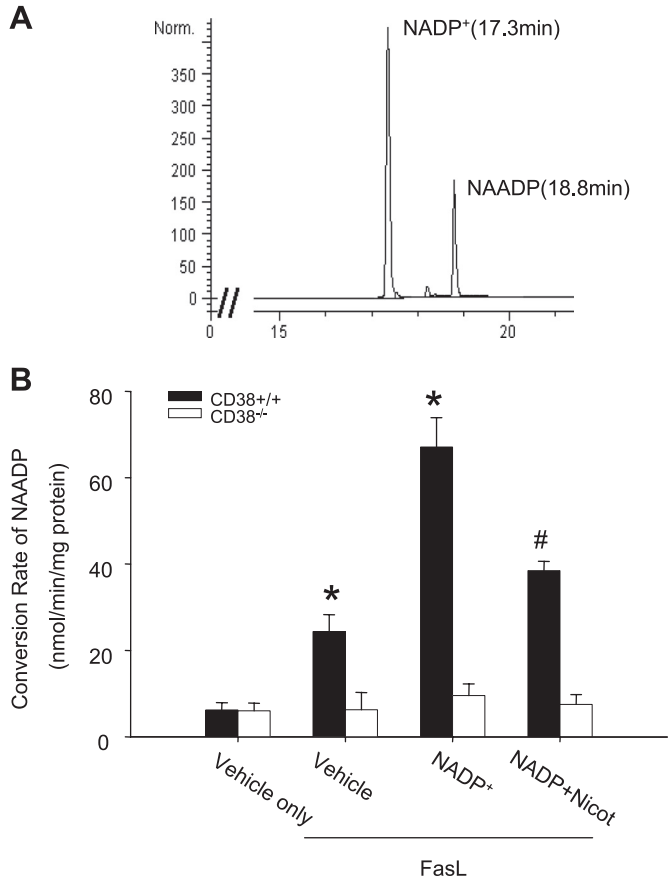

Fig. 2. HPLC analysis of nicotinic acid adenine dinucleotide phosphate (NAADP) conversion rate in CAMs. *A*: typical chromatogram of $NADP^+$ and NAADP. *B*: conversion rate of $NADP^+$ to NAADP in $CD38^{+/+}$ and $CD38^{-/-}$ CAMs under Fas ligand (FasL; 10 ng/ml) in the presence or absence of the CD38 inhibitor nicotinamide (Nicot; 6 mM). Values are means ± SE ($n = 6$ experiments). *$P < 0.05$ vs. vehicle only. #$P < 0.05$ vs. $NADP^+$ group.

tration of 5 μM. Ca^{2+} release and lysosome trace recordings were performed with FasL (10 ng/ml) treatment following the method previously in *Confocal fluorescence microscopic $[Ca^{2+}]_i$ measurement*. Lysosome/Rho (Lyso/Rho) fluorescence images were acquired at 568-nm excitation and 590-nm emission. The colocalization coefficiency of Ca^{2+}/fluo-4 and Lyso/Rho was analyzed with Image-Pro Plus 6.0 software (44).

Isolated small artery tension recording. Small ventricular septal arteries (~150-μm inner diameter) were dissected (28) and then mounted in a Multi Myograph 610M (Danish Myo Technology, Aarhus, Denmark) for recording of isometric wall tension (6, 8) after 30 min of equilibration in physiological saline solution (PSS; pH 7.4) containing (in mM) 119 NaCl, 4.7 KCl, 1.6 $CaCl_2$, 1.17 $MgSO_4$ 1.18 NaH_2PO_4, 2.24 $NaHCO_3$, 0.026 EDTA, and 5.5 glucose at 37°C bubbled with a gas mixture of 95% O_2 and 5% CO_2. After basic tension was set, the dose effect of FasL alone (1, 3, 10, and 30 ng/ml) to the tension changes of the septal arterial wall were measured. In other group experiments, the arteries were precontracted with a thromboxane A_2 analog, U-46619 (50 nM; Sigma, St. Louis, MO), and the dose effect of FasL vasoconstriction was reexamined with or without the presence of different inhibitors: Baf (100 nM), Rya (50 μM), or 2-aminoethoxydiphenyl borate (2-APB; 100 μM). The time-course effects of FasL (30 ng/ml) alone and FasL (30 ng/ml) plus U-46619 (50 nM) on vasoconstriction were examined in both wild-type and $CD38^{-/-}$ arteries.

Statistics. Data are means ± SE. Significant differences between and within multiple groups were examined using ANOVA for repeated measurements, followed by Duncan's multiple-range test. Student's *t*-test was used to evaluate the significant difference between two groups of observations. $P < 0.05$ was considered statistically significant.

RESULTS

Genotyping of CD38 knockout mice and identity confirmation of isolated CAMs. Figure 1*A* depicts a PCR product gel document from genotyping experiments. It shows that CD38 gene-specific PCR product (299 bp) from extron 2 was amplified from wild-type mice (*lane 1*) but not from CD38 knockout ($CD38^{-/-}$) mice [*lane 2* or *3* (male) and *lane 4* or *5* (female)]. Neomycin-resistant gene cassette (Neo)-specific PCR product (280 bp) was amplified from $CD38^{-/-}$ mice [*lane 7* or *8* (male) and *lane 9* (female)] but not from $CD38^{+/+}$ mice (*lane 6*). In Fig. 1*B*, the CAMs' identity was confirmed by positive staining with the anti-α-smooth muscle actin primary antibody and Alexa-Fluor 488-conjugated anti-mouse IgG secondary anti-

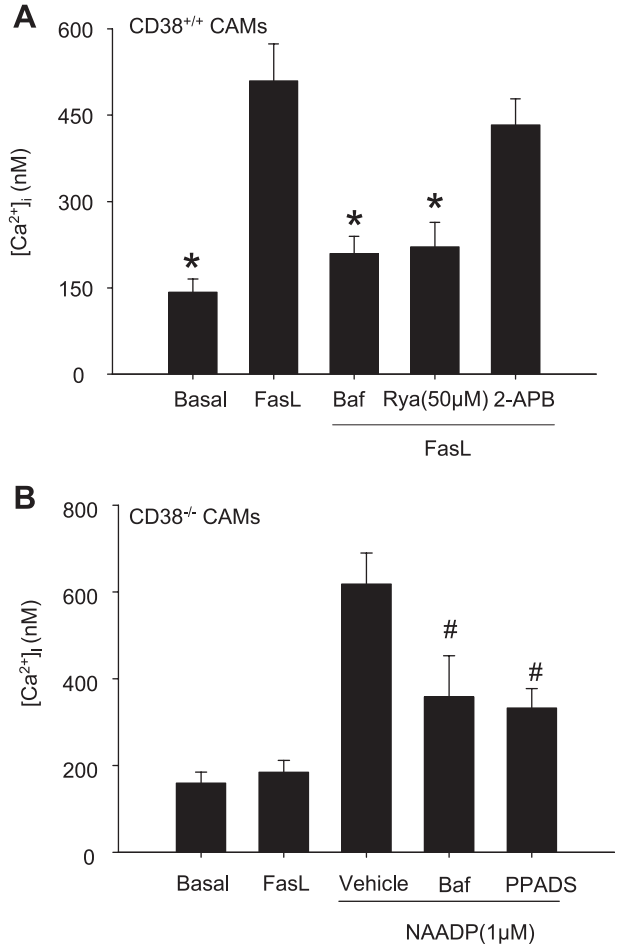

Fig. 3. FasL induced Ca^{2+} release in mouse CAMs as shown by fluorescent Ca^{2+} imaging analysis. *A*: intracellular Ca^{2+} responses to FasL (10 ng/ml) in the absence or presence of bafilomycin A1 (Baf; 100 nM), ryanodine (Rya; 50 μM), or 2-aminoethoxydiphenyl borate (2-APB; 100 μM) in CAMs from wild-type ($CD38^{+/+}$) mice. *B*: intracellular Ca^{2+} response to FasL (10 ng/ml) or NAADP (1 μM) with or without pretreatment with Baf (100 nM) or pyridoxalphosphate-6-azophenyl-2-disulfonic acid (PPADS; 50 μM) in CAMs from $CD38^{-/-}$ mice. Values are means ± SE ($n = 6$ experiments). *$P < 0.05$ vs. FasL group. #$P < 0.05$ vs. vehicle group.

body; endothelial cells were used as control (negative staining).

Production of NAADP in CAMs. Using HPLC analysis, we first determined whether CD38 acted as an enzyme responsible for NAADP production by measuring NAADP conversion rate from its substrate, $NADP^+$, in CAMs isolated from wild-type and $CD38^{-/-}$ mice. Figure 2*A* presents a representative reversed-phase HPLC chromatogram depicting the profile of $NADP^+$ and its CD38 enzymatic metabolite, NAADP. Figure 2*B* summarizes the effects of CD38 genotype on the NAADP production. FasL markedly increased the NAADP conversion rate in wild-type CAMs from 6.2 ± 1.7 nmol·min^{-1}·mg protein^{-1} of vehicle to 24.3 ± 3.9 nmol·min^{-1}·mg protein^{-1} in the presence of FasL and 67.1 ± 6.8 nmol·min^{-1}·mg protein^{-1} with $NADP^+$ plus FasL. This NAADP conversion activity could be significantly attenuated by nicotinamide, a specific CD38 inhibitor. In contrast, the NAADP conversion rate had no change even though FasL was used for stimulation in $CD38^{-/-}$ CAMs, whether the substrate of $NADP^+$ was added or not.

Lack of FasL-induced Ca^{2+} release in CAMs from $CD38^{-/-}$ mice. In these experiments, the Ca^{2+} release response to FasL between the wild-type and $CD38^{-/-}$ CAMs was compared. As shown in Fig. 3*A*, in wild-type CAMs, FasL (10 ng/ml) significantly increased $[Ca^{2+}]_i$ release (509.4 ± 64.3 vs. 142.5 ± 22.5 nM at the basal level), and this Ca^{2+} response to FasL was almost abolished by the lysosome function inhibitor Baf or the SR Rya/Ca^{2+} channel inhibitor Rya (50 μM). Baf is a lysosomal vacuolar H^+-ATPase antagonist; inhibition of vacuolar H^+-ATPase would deenergize H^+/Ca^{2+} exchanger and Ca^{2+} sequestering into lysosomes (42), which would lead to lysosomal Ca^{2+} depletion and result in no Ca^{2+} release response from lysosomes upon FasL stimulation. However, the Ca^{2+} release response to FasL was not affected by 2-APB (100 μM), a SR IP_3 receptor/Ca^{2+} antagonist. In contrast, FasL failed to release Ca^{2+} in CAMs from $CD38^{-/-}$ mice. If NAADP (1 μM) was directly introduced into the cells, Ca^{2+} release occurred (618.7 ± 70.8 vs. 159.7 ± 25.1 nM at the basal level). This effect of intracellular NAADP delivery was attenuated by Baf (100 nM) or the NAADP antagonist pyridoxalphosphate-6-azophenyl-2-disulfonic acid (50 μM) (Fig. 3*B*).

CD38 plasmid transfection rescued FasL-induced Ca^{2+} release response in CAMs of $CD38^{-/-}$ mice. To further examine the role of CD38 in FasL-induced Ca^{2+} release, we transferred CD38/GFP gene back to $CD38^{-/-}$ CAMs and then measured the Ca^{2+} response to FasL. In Fig. 4*A*, the green fluorescence in the cells at *left* shows positive expression of the CD38 transgene. The light microscopic image (*middle*) shows the number of cells. The merged image at *right* shows that the CD38 transfection efficiency was over 85% cells. In Fig. 4*B*, the summarized results show that FasL had no Ca^{2+} release effect in $CD38^{-/-}$ cells as detected before. However, in the CD38 gene rescued cells, FasL-induced Ca^{2+} response was restored to a level comparable to that observed in wild-type cells (441.79 ± 35.53 vs. 521.73 ± 61.08 nM).

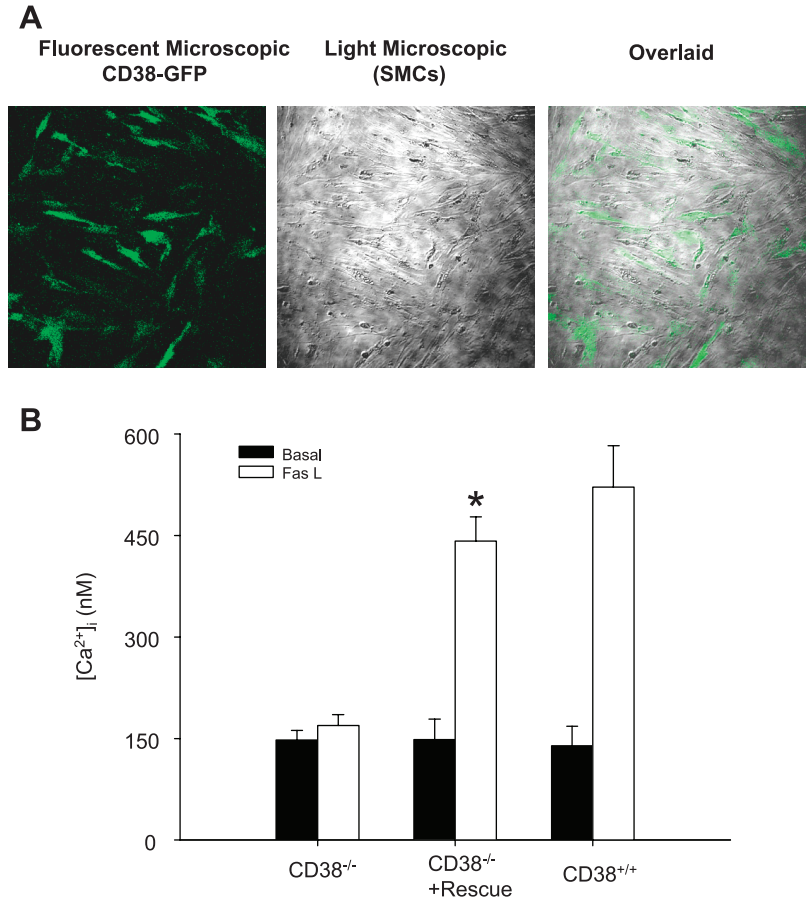

Fig. 4. CD38 plasmid transfection rescued FasL-induced Ca^{2+} release in CAMs of $CD38^{-/-}$ mice. *A*: confirmation of CD38/green fluorescent protein (GFP) transfection in CAMs. SMCs, smooth muscle cells. *B*: FasL-induced Ca^{2+} response in CD38-rescued CAMs was restored to the level in that of $CD38^{+/+}$ CAMs. Values are means ± SE ($n = 6$ experiments). *$P < 0.05$ vs. $CD38^{-/-}$ group.

Confocal microscopic analysis of FasL-induced two-phase Ca^{2+} release in CAMs from CD38$^{+/+}$ mice. Using confocal microscopic analysis, we further explored the mechanism underlying the two-phase Ca^{2+} response in CAMs from wild-type mice. In Fig. 5*A*, representative sequential images showed a dynamic response of intracellular Ca^{2+} upon FasL (10 ng/ml) stimulation. The color scale from blue to red reflects the intracellular Ca^{2+} release. After FasL (10 ng/ml) treatment, a first-phase Ca^{2+} release from the basal level was observed at 4.5 min (local red image), followed by a second-phase Ca^{2+} wave at 10 min (whole cell red image). In CAMs pretreated with the SR Ca^{2+} release inhibitor Rya (50 μM), the second Ca^{2+} release phase was abolished, but the first Ca^{2+} release phase remained the same. However, after treatment with the lysosomal inhibitor Baf, both of the first- and second-phase Ca^{2+} releases were no longer observed (Supplemental Result 1). (Supplemental data for this article is available online at the *American Journal of Physiology-Cell Physiology* website.) Furthermore, in CD38$^{-/-}$ cells, this two-phase Ca^{2+} release could not be detected by FasL (data not shown). Figure 5*B* summarizes the FasL-induced two-phase Ca^{2+} release in CAMs of CD38$^{+/+}$ mice. The ratio of Ca^{2+}-dependent fluorescence intensity to the basal level was quantified to present the intracellular Ca^{2+} release response. In the control group, the Ca^{2+} intensity ratio was significantly increased by 75% at the first phase and 1.4-fold at the second phase after FasL (10 ng/ml) treatment. However, in the presence of Rya (50 μM), the Ca^{2+} release of the second phase was substantially attenuated, whereas the Ca^{2+} intensity ratio in the first phase remained the same as in the control group. Furthermore, when the cells were pretreated with Baf, Ca^{2+} release of both the first and second phase was totally abolished.

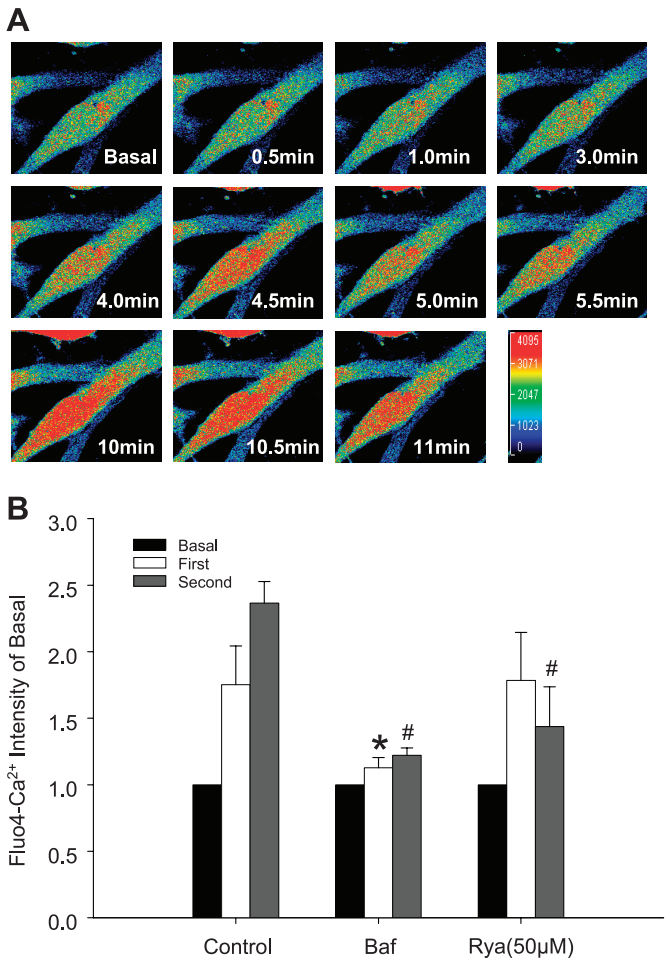

Fig. 5. Confocal microscopic analysis of FasL-induced 2-phase Ca^{2+} release in CAMs of CD38$^{+/+}$. *A*: sequential images of intracellular Ca^{2+} response to FasL (10 ng/ml) with the fluorescence indicator fluo-4. The occurrence of color from green to red represents Ca^{2+} release. *B*: FasL-induced 2-phase Ca^{2+} release in CAMs of CD38$^{+/+}$ in the presence or absence of Baf (100 nM) or Rya (50 μM). The ratio of Ca^{2+}-dependent fluorescence intensity to basal level was quantified to present the intracellular Ca^{2+} release response. Values are means ± SE (n = 6 experiments). *$P < 0.05$ vs. first phase in control group. #$P < 0.05$ vs. second phase in control group.

To further confirm that the first-phase Ca^{2+} release was derived from lysosomes upon FasL (10 ng/ml) stimulation, we performed lysosome and Ca^{2+} release colocalization experiments. The confocal microscopic images (Fig. 6*A*) demonstrate that the Ca^{2+} release in the first phase(4.5 min) appeared as an unevenly Ca^{2+}-sparking image (green image, Ca^{2+}/fluo-4), and the highest Ca^{2+} release regions were colocalized well with lysosomes (red image, Lyso/Rho), which resulted in strong yellow spots (overlay). In contrast, the subsequent global Ca^{2+} release in second phase (10.0 min) was evenly distributed within the whole cell, and no specific regional yellow spots were observed. The colocalization coefficiency of Ca^{2+}/fluo-4 and Lyso/Rho in basal, first-phase (4.5 min), and second-phase (10.0 min) Ca^{2+} release was 0.183 ± 0.056, 0.414 ± 0.102, and 0.288 ± 0.041, respectively (Fig. 6*B*). These colocalization results provide direct evidence that the lysosomes act as Ca^{2+} stores for the first-phase Ca^{2+} release in response to FasL activation.

FasL increased coronary arterial vasoconstrictor response to U-46619 in CD38$^{+/+}$ but not in CD38$^{-/-}$ mice. To investigate physiological relevance of FasL-associated two-phase Ca^{2+} release, we used the coronary arteries from both CD38$^{-/-}$ and wild-type mice to record arterial tension changes. In Fig. 7*A*, FasL-induced percent increases in U-46619-induced vasoconstriction were dose dependent by a maximum of 82.3 ± 5.3% at the dose of 30 ng/ml used. In contrast, this FasL-induced arterial constriction enhancement was not detected in CD38$^{-/-}$ mice. It should be noted that FasL alone had no vasoconstriction effects in both types of arteries. In Fig. 7, *B* and 7C, after blocking of SR Ca^{2+} release by Rya (50 μM) or lysosomal function by Baf, wild-type arteries lost vasoconstriction, whereas CD38$^{-/-}$ arteries showed no change. Pretreatment of the arteries with the IP_3 antagonist 2-APB had no effect in blocking vasoconstriction in both types of arteries (Fig. 7*D*). The time-course dynamic tension recording traces revealed that FasL (30 ng/ml) effectively enhanced U-46619 (50 nM)-induced vessel constriction in wild-type artery, with a similar time frame to that observed in the CAM Ca^{2+} release study. Consistent with the dose-effect data obtained from vasoconstriction analysis, the time-course results also indicate that FasL alone had no vessel constriction effects, as well as no vessel constriction enhancement effects, in CD38$^{-/-}$ artery (Supplemental Result 2).

DISCUSSION

The present study has demonstrated that CD38 is the enzyme responsible for the FasL-induced NAADP production and that CD38/NAADP pathway is involved in the FasL-induced Ca^{2+}

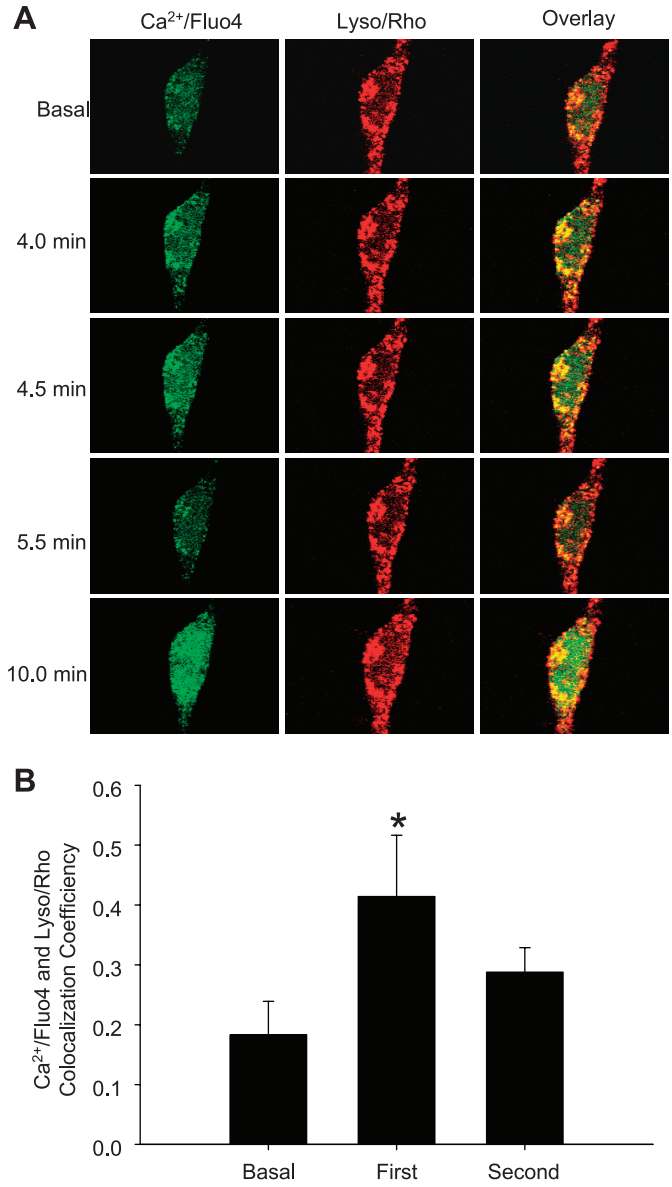

Fig. 6. Confocal microscopic confirmation of first-phase Ca^{2+} release from lysosomes in CAMs of $CD38^{+/+}$. *A*: sequential images show that the Ca^{2+} release in the first phase (4.5 min) appeared as an unevenly Ca^{2+}-sparking image (green images in Ca^{2+}/fluo-4), and the highest Ca^{2+} release regions were colocalized well with lysosomes/rhodamine (red images in Lyso/Rho), which resulted in strong yellow spots (overlay). In contrast, the subsequent global Ca^{2+} release in the second phase (10 min) was evenly distributed within the whole cell, and no specific regional yellow spots were observed. *B*: summarized results showed colocalization coefficiency of Ca^{2+}/fluo-4 and Lyso/Rho at the basal level, first-phase (4.5 min), and second-phase (10 min) Ca^{2+} releases, respectively. Values are means ± SE (n = 6 experiments). *$P < 0.05$ vs. other groups.

release response in CAMs. This FasL-induced increase in $[Ca^{2+}]_i$ through activation of NAADP signaling pathway is associated with a two-phase Ca^{2+} release from lysosomes and then SR stores. Functionally, the two-phase Ca^{2+} response to FasL importantly contributes to vasoconstriction in coronary artery.

Using CD38 knockout mice and HPLC analysis, we have found that CD38 is the enzyme responsible for FasL-associated NAADP production in coronary artery by measuring the NAADP conversion rate. This result is in agreement with previous findings that CD38 is the major enzyme for the NAADP synthesis in vitro (1, 27, 43). Although there was a report that expression of CD38 did not correlate with in vivo intracellular NAADP concentration (34), our results clearly demonstrated that FasL only increased NAADP production in wild-type but not $CD38^{-/-}$ mouse coronary arteries, whether additional exogenous substrates of $NADP^+$ and NA were presented or not. Furthermore, our functional studies demonstrated that rescued CD38 expression in the $CD38^{-/-}$ CAMs could restore the FasL-induced Ca^{2+} response to the level of wild-type cells. These results provide direct evidence that CD38 plays a critical role in producing NAADP in response to

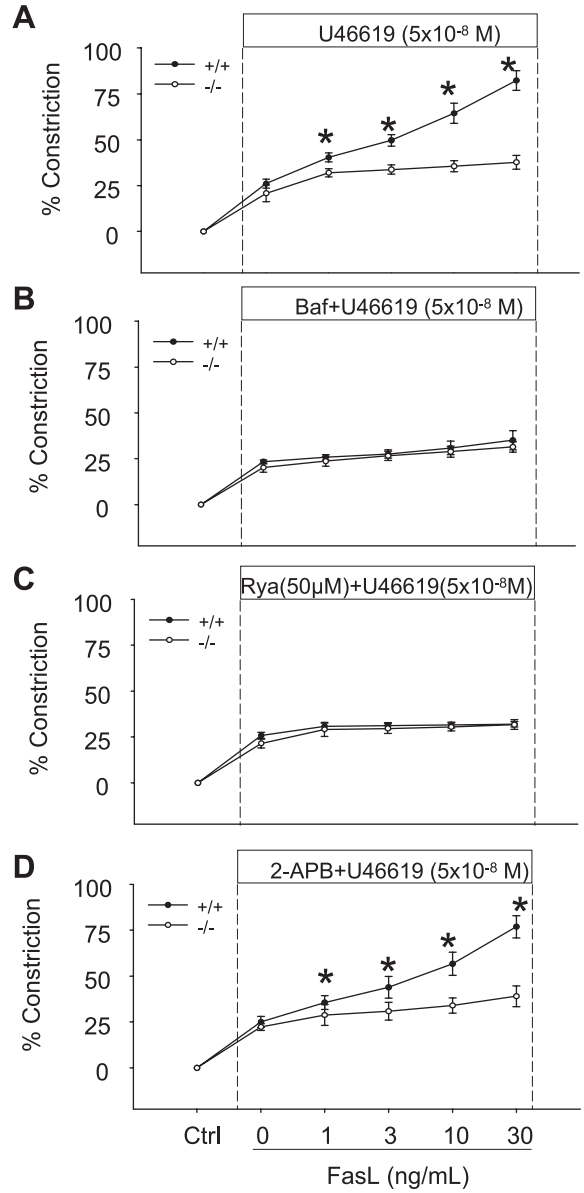

Fig. 7. FasL increased the coronary artery vasoconstriction response to U-46619 in $CD38^{+/+}$ but not $CD38^{-/-}$ mice. *A*: effects of FasL on U-46619-induced vasoconstriction in coronary arteries from $CD38^{+/+}$ (+/+) and $CD38^{-/-}$ (−/−) mice under FasL (10 ng/ml) treatment. *B–D*: this FasL-sensitized vasoconstrictor effect was almost blocked by pretreatment with the lysosomal function inhibitor Baf (100 nM; *B*) or the SR Rya/Ca^{2+} antagonist Rya (50 μM; *C*), but not by the IP_3 receptor antagonist 2-APB (100 μM; *D*). Values are means ± SE (n = 6 experiments). *$P < 0.05$ vs. $CD38^{-/-}$ group.

FasL in coronary arteries. It should be noted that some other enzymatic pathways for the synthesis of NAADP also have been proposed. For example, ADP-ribosyl cyclase was reported to convert cADPR and nicotinic acid to NAADP (29), and CD157 as a member of the CD38 family has been found to be responsible for NAADP production in some tissues or cells (31). In addition, NAADP can be formed via NAD kinase (32) by conversion of amide to acid in NADP or by phosphorylation of NADP as well as via NAD(P)H oxidase to convert NAADPH to NAADP (3). Although not yet extensively studied, it is possible that these different enzymatic pathways may be tissue specific and exert their action under different physiological or pathological conditions. In regard to the possible mechanism by which FasL activates CD38 to generate NAADP, our recent studies have reported that CD38 could be aggregated in membrane raft clusters in coronary arterial smooth muscle cells and thereby result in the increased activity of CD38 as ADP-ribosyl cyclase for cADPR generation (22). Given that FasL is a potent stimulator for production of ceramide, a pivotal molecular for membrane raft clustering (40), it is possible that FasL stimulates ceramide production and consequently results in membrane raft clustering with CD38 aggregation and activation.

One of the important findings in the present study is that FasL, a TNF family member, could induce lysosome-dependent Ca^{2+} release through NAADP. Our confocal microscopic analysis revealed that FasL initiated local Ca^{2+} burst from lysosomes and then generated global Ca^{2+} wave from the SR, a two-phase Ca^{2+} release response that was observed in NAADP-mediated Ca^{2+} signaling by ET-1 in smooth muscle cells (24, 43). It should be noted that the time interval between two phases of Ca^{2+} release in response to FasL or ET-1 was about 3–5 min, which is much longer than the time taken by classic CICR that usually occurs in seconds. Although there is no direct evidence to explain why and how the second phase of Ca^{2+} release takes so long, some recent advances in lysosomal function studies may shed some light on this enigma. Lysosomes are membrane-bound organelles that primarily serve as catabolic compartments in eukaryotic cells (14). After maturation, lysosomes are consistently undergoing heterotypic fusion with endocytic vesicles for degradation of internalized molecules (12) and homotypic fusion for redistribution of lysosomal contents (21), which is dependent on lysosome-associated movement (2). Given such innate dynamic properties of lysosomes, it is possible that the first phase Ca^{2+} release will drive lysosome aggregation and/or movement to the SR and then trigger a global Ca^{2+} wave, and this lysosome movement or aggregation may contribute to such a long time interval between two-phase Ca^{2+} responses. Along this line, it is hypothesized that FasL binds to Fas to activate lysosome Ca^{2+} bursts; such small bursts may not be enough to activate global Ca^{2+} release from the SR, but rather activate lysosome movement or aggregation. When lysosomes aggregate more or move close to the SR, the global Ca^{2+} release is activated. However, this assumption needs to be further verified.

Functionally, FasL have been demonstrated to be a proinflammatory factor that is implicated in the pathophysiological process of various cardiovascular diseases such as coronary heart disease, arteriosclerosis, and ischemia-reperfusion injury (15, 20, 33). Although the role of Fas/FasL-mediated apoptosis has been well elaborated in those vascular disorders, little is known about the vascular early response to Fas activation. In the present studies, in addition to cell studies on Ca^{2+} response, we also performed arterial tension recording experiments to explore the early function change during Fas activation. We found that FasL enhanced U-46619-induced vasoconstriction in wild-type mouse artery and that this vasoconstriction response was consistent with a time frame of the FasL-induced two-phase Ca^{2+} response as observed in the Ca^{2+} release of CAMs. Obviously, this FasL-induced slow vasomotor response is different from that of instant vasoconstriction provoked by some classic vasoactive agonists (e.g., norepinephrine, angiotensin II, or ATP), which are dependent on the PLC-mediated direct Ca^{2+} release from the SR. This two-phase Ca^{2+} release and slow vasoconstriction may be an important mechanism maintaining vascular tone, and therefore NAADP signaling pathway in vascular smooth muscle may be critical for the development of sustained vascular tone. This hypothesis needs to be further tested. In addition, a chronic elevation of intracellular Ca^{2+} in vascular smooth muscles also may produce histopathological alterations that may finally lead to severe consequences such as vascular remodeling and arteriosclerotic lesion (16).

In summary, the present study demonstrated that *1*) CD38 was the major enzyme responsible for the production of NAADP in response to FasL activation; *2*) FasL initiated Ca^{2+} release through lysosomal NAADP Ca^{2+} pathway; *3*) the NAADP-induced two-phase Ca^{2+} response to FasL was associated with lysosome Ca^{2+}-triggering action and subsequent CICR, which resulted in a large global increase in $[Ca^{2+}]_i$; and *4*) the lysosome-associated Ca^{2+} regulatory mechanism through NAADP participated in the coronary vasoconstriction response to FasL. We have concluded that FasL activated lysosome/NAADP Ca^{2+} pathway and led to vasoconstriction in the coronary artery, which might represent the early response of Fas activation in the cardiovascular system.

GRANTS

This work was supported by National Heart, Lung, and Blood Institute Grants HL057244 and HL091464.

DISCLOSURES

No conflicts of interest are declared by the authors.

REFERENCES

1. **Aarhus R, Graeff RM, Dickey DM, Walseth TF, Lee HC.** ADP-ribosyl cyclase and CD38 catalyze the synthesis of a calcium-mobilizing metabolite from NADP. *J Biol Chem* 270: 30327–30333, 1995.
2. **Andrews NW.** Regulated secretion of conventional lysosomes. *Trends Cell Biol* 10: 316–321, 2000.
3. **Billington RA, Thuring JW, Conway SJ, Packman L, Holmes AB, Genazzani AA.** Production and characterization of reduced NAADP (nicotinic acid-adenine dinucleotide phosphate). *Biochem J* 378: 275–280, 2004.
4. **Boittin FX, Galione A, Evans AM.** Nicotinic acid adenine dinucleotide phosphate mediates Ca^{2+} signals and contraction in arterial smooth muscle via a two-pool mechanism. *Circ Res* 91: 1168–1175, 2002.
5. **Brailoiu E, Churamani D, Cai X, Schrlau MG, Brailoiu GC, Gao X, Hooper R, Boulware MJ, Dun NJ, Marchant JS, Patel S.** Essential requirement for two-pore channel 1 in NAADP-mediated calcium signaling. *J Cell Biol* 186: 201–209, 2009.
6. **Brandin L, Bergstrom G, Manhem K, Gustafsson H.** Oestrogen modulates vascular adrenergic reactivity of the spontaneously hypertensive rat. *J Hypertens* 21: 1695–1702, 2003.
7. **Bright NA, Gratian MJ, Luzio JP.** Endocytic delivery to lysosomes mediated by concurrent fusion and kissing events in living cells. *Curr Biol* 15: 360–365, 2005.

8. **Bund SJ, Lee RM.** Arterial structural changes in hypertension: a consideration of methodology, terminology and functional consequence. *J Vasc Res* 40: 547–557, 2003.
9. **Calcraft PJ, Ruas M, Pan Z, Cheng X, Arredouani A, Hao X, Tang J, Rietdorf K, Teboul L, Chuang KT, Lin P, Xiao R, Wang C, Zhu Y, Lin Y, Wyatt CN, Parrington J, Ma J, Evans AM, Galione A, Zhu MX.** NAADP mobilizes calcium from acidic organelles through two-pore channels. *Nature* 459: 596–600, 2009.
10. **Churchill GC, Galione A.** NAADP induces Ca^{2+} oscillations via a two-pool mechanism by priming IP_3- and cADPR-sensitive Ca^{2+} stores. *EMBO J* 20: 2666–2671, 2001.
11. **Churchill GC, Okada Y, Thomas JM, Genazzani AA, Patel S, Galione A.** NAADP mobilizes Ca^{2+} from reserve granules, lysosome-related organelles, in sea urchin eggs. *Cell* 111: 703–708, 2002.
12. **Clague MJ.** Molecular aspects of the endocytic pathway. *Biochem J* 336: 271–282, 1998.
13. **Dammermann W, Guse AH.** Functional ryanodine receptor expression is required for NAADP-mediated local Ca^{2+} signaling in T-lymphocytes. *J Biol Chem* 280: 21394–21399, 2005.
14. **De Duve C, Wattiaux R.** Functions of lysosomes. *Annu Rev Physiol* 28: 435–492, 1966.
15. **Feng QZ, Zhao YS, Abdelwahid E.** The role of Fas in the progression of ischemic heart failure: prohypertrophy or proapoptosis. *Coron Artery Dis* 19: 527–534, 2008.
16. **Fleckenstein-Grun G, Frey M, Thimm F, Hofgartner W, Fleckenstein A.** Calcium overload–an important cellular mechanism in hypertension and arteriosclerosis. *Drugs* 44, *Suppl* 1: 23–30, 1992.
17. **Gerasimenko JV, Maruyama Y, Yano K, Dolman NJ, Tepikin AV, Petersen OH, Gerasimenko OV.** NAADP mobilizes Ca^{2+} from a thapsigargin-sensitive store in the nuclear envelope by activating ryanodine receptors. *J Cell Biol* 163: 271–282, 2003.
18. **Graeff R, Liu Q, Kriksunov IA, Hao Q, Lee HC.** Acidic residues at the active sites of CD38 and ADP-ribosyl cyclase determine nicotinic acid adenine dinucleotide phosphate (NAADP) synthesis and hydrolysis activities. *J Biol Chem* 281: 28951–28957, 2006.
19. **Grynkiewicz G, Poenie M, Tsien RY.** A new generation of Ca^{2+} indicators with greatly improved fluorescence properties. *J Biol Chem* 260: 3440–3450, 1985.
20. **Henriques-Pons A, de Oliveira GM.** Is the Fas/Fas-L pathway a promising target for treating inflammatory heart disease? *J Cardiovasc Pharmacol* 53: 94–99, 2009.
21. **Heuser J.** Changes in lysosome shape and distribution correlated with changes in cytoplasmic pH. *J Cell Biol* 108: 855–864, 1989.
22. **Jia SJ, Jin S, Zhang F, Yi F, Dewey WL, Li PL.** Formation and function of ceramide-enriched membrane platforms with CD38 during M1-receptor stimulation in bovine coronary arterial myocytes. *Am J Physiol Heart Circ Physiol* 295: H1743–H1752, 2008.
23. **Kavurma MM, Bennett MR.** Expression, regulation and function of trail in atherosclerosis. *Biochem Pharmacol* 75: 1441–1450, 2008.
24. **Kinnear NP, Boittin FX, Thomas JM, Galione A, Evans AM.** Lysosome-sarcoplasmic reticulum junctions. A trigger zone for calcium signaling by nicotinic acid adenine dinucleotide phosphate and endothelin-1. *J Biol Chem* 279: 54319–54326, 2004.
25. **Lee HC.** Physiological functions of cyclic ADP-ribose and NAADP as calcium messengers. *Annu Rev Pharmacol Toxicol* 41: 317–345, 2001.
26. **Lee HC, Aarhus R.** A derivative of NADP mobilizes calcium stores insensitive to inositol trisphosphate and cyclic ADP-ribose. *J Biol Chem* 270: 2152–2157, 1995.
27. **Liang M, Chini EN, Cheng J, Dousa TP.** Synthesis of NAADP and cADPR in mitochondria. *Arch Biochem Biophys* 371: 317–325, 1999.
28. **Lui AH, McManus BM, Laher I.** Endothelial and myogenic regulation of coronary artery tone in the mouse. *Eur J Pharmacol* 410: 25–31, 2000.
29. **Moreschi I, Bruzzone S, Melone L, De Flora A, Zocchi E.** $NAADP^+$ synthesis from cADPRP and nicotinic acid by ADP-ribosyl cyclases. *Biochem Biophys Res Commun* 345: 573–580, 2006.
30. **Ohta S, Suzuki K, Tachibana K, Yamada G.** Microbubble-enhanced sonoporation: efficient gene transduction technique for chick embryos. *Genesis* 37: 91–101, 2003.
31. **Ortolan E, Vacca P, Capobianco A, Armando E, Crivellin F, Horenstein A, Malavasi F.** CD157, the Janus of CD38 but with a unique personality. *Cell Biochem Funct* 20: 309–322, 2002.
32. **Palade P.** The hunt for an alternate way to generate NAADP. Focus on "NAADP as a second messenger: neither CD38 nor base-exchange reaction are necessary for in vivo generation of NAADP in myometrial cells." *Am J Physiol Cell Physiol* 292: C4–C7, 2007.
33. **Sata M, Suhara T, Walsh K.** Vascular endothelial cells and smooth muscle cells differ in expression of Fas and Fas ligand and in sensitivity to Fas ligand-induced cell death: implications for vascular disease and therapy. *Arterioscler Thromb Vasc Biol* 20: 309–316, 2000.
34. **Soares S, Thompson M, White T, Isbell A, Yamasaki M, Prakash Y, Lund FE, Galione A, Chini EN.** NAADP as a second messenger: neither CD38 nor base-exchange reaction are necessary for in vivo generation of NAADP in myometrial cells. *Am J Physiol Cell Physiol* 292: C227–C239, 2007.
35. **Taniyama Y, Tachibana K, Hiraoka K, Namba T, Yamasaki K, Hashiya N, Aoki M, Ogihara T, Yasufumi K, Morishita R.** Local delivery of plasmid DNA into rat carotid artery using ultrasound. *Circulation* 105: 1233–1239, 2002.
36. **Teng B, Ansari HR, Oldenburg PJ, Schnermann J, Mustafa SJ.** Isolation and characterization of coronary endothelial and smooth muscle cells from A_1 adenosine receptor-knockout mice. *Am J Physiol Heart Circ Physiol* 290: H1713–H1720, 2006.
37. **Vecchione C, Frati A, Di Pardo A, Cifelli G, Carnevale D, Gentile MT, Carangi R, Landolfi A, Carullo P, Bettarini U, Antenucci G, Mascio G, Busceti CL, Notte A, Maffei A, Cantore GP, Lembo G.** Tumor necrosis factor-alpha mediates hemolysis-induced vasoconstriction and the cerebral vasospasm evoked by subarachnoid hemorrhage. *Hypertension* 54: 150–156, 2009.
38. **Wainwright CL, Miller AM, Wadsworth RM.** Inflammation as a key event in the development of neointima following vascular balloon injury. *Clin Exp Pharmacol Physiol* 28: 891–895, 2001.
39. **Zhang AY, Yi F, Teggatz EG, Zou AP, Li PL.** Enhanced production and action of cyclic ADP-ribose during oxidative stress in small bovine coronary arterial smooth muscle. *Microvasc Res* 67: 159–167, 2004.
40. **Zhang AY, Yi F, Zhang G, Gulbins E, Li PL.** Lipid raft clustering and redox signaling platform formation in coronary arterial endothelial cells. *Hypertension* 47: 74–80, 2006.
41. **Zhang F, Jin S, Yi F, Li PL.** TRP-ML1 functions as a lysosomal NAADP-sensitive Ca^{2+} release channel in coronary arterial myocytes. *J Cell Mol Med* 13: 3174–3185, 2009.
42. **Zhang F, Li PL.** Reconstitution and characterization of a nicotinic acid adenine dinucleotide phosphate (NAADP)-sensitive Ca^{2+} release channel from liver lysosomes of rats. *J Biol Chem* 282: 25259–25269, 2007.
43. **Zhang F, Zhang G, Zhang AY, Koeberl MJ, Wallander E, Li PL.** Production of NAADP and its role in Ca^{2+} mobilization associated with lysosomes in coronary arterial myocytes. *Am J Physiol Heart Circ Physiol* 291: H274–H282, 2006.
44. **Zinchuk V, Zinchuk O, Okada T.** Quantitative colocalization analysis of multicolor confocal immunofluorescence microscopy images: pushing pixels to explore biological phenomena. *Acta Histochem Cytochem* 40: 101–111, 2007.